Kinetics of swelling under constraint

Qihan Liu, Agathe Robisson, Yucun Lou, and Zhigang Suo

Citation: J. Appl. Phys. **114**, 064901 (2013); doi: 10.1063/1.4816337
View online: http://dx.doi.org/10.1063/1.4816337
View Table of Contents: http://jap.aip.org/resource/1/JAPIAU/v114/i6
Published by the AIP Publishing LLC.

Kinetics of swelling under constraint

Qihan Liu,[1] Agathe Robisson,[2] Yucun Lou,[2,a)] and Zhigang Suo[1]
[1]*School of Engineering and Applied Sciences, Harvard University, Cambridge, Massachusetts 02138, USA*
[2]*Schlumberger-Doll Research, One Hampshire Street, Cambridge, Massachusetts 02139, USA*

(Received 10 June 2013; accepted 2 July 2013; published online 8 August 2013)

Swellable elastomers are used to seal flow channels in oilfield operations. After sealing, the elastomers are constrained triaxially, and a contact load builds up between the elastomers and surrounding rigid materials. For these applications, the ability to predict the evolution of the contact load is important. This work introduces an experimental setup to measure the contact load as a function of time. The experimental data are well represented by a simple time-relaxation equation derived from the linear poroelastic theory, enabling a determination of the effective diffusivity of solvent inside the elastomers. © *2013 AIP Publishing LLC*. [http://dx.doi.org/10.1063/1.4816337]

I. INTRODUCTION

A swellable elastomer is a cross-linked polymer network that can imbibe solvent, resulting in an increase in volume when the polymer is free to swell, and a development of force when the polymer is constrained by the surrounding materials. The swelling is used in applications in oilfields, e.g., as self-healing cements[1–3] and swellable packers.[4–7] In an application, the elastomer is selected to imbibe a certain kind of fluid (water, oil, or natural gas), called the solvent. Whenever exposed to the solvent, the elastomer will swell and seal the flow channel. Such a seal is self-actuated, which is attractive for applications where interventions are expensive or time-consuming. For a self-healing cement, small elastomer particles are incorporated into the cement. When the cement cracks, the elastomer particles are exposed to the downhole fluid, swell and seal the cracks. For a swellable packer, a cylindrical tube of an elastomer imbibes the downhole fluid, swells, and seals the wellbore.

In these oilfield applications, the swelling is under triaxially constrained conditions. In the self-healing cement, the elastomer particles are constrained by the cement matrix. In the elastomer packer, the cylindrical tube is constrained by the metallic casing and rocks. A compressive load, known as swelling pressure, will develop against the constraints. In general, the larger the swelling pressure, the better the seal. The time to build up the swelling pressure is also critical for these applications. For example, the cement is required to firmly bond with casing and rocks after several days,[8,9] and the swellable packer is required to sustain a large differential pressure after several weeks.[10,11]

There are many studies on swellable elastomers under free-swelling conditions (e.g., Refs. 12–14), but little work has been done to measure the buildup of swelling pressure under constraints. Several nonlinear field theories have been developed in the past few years.[15–18] After characterizing the parameters in the theories using experiments with simple boundary conditions, these theories in principle can be used to predict the behavior of swellable elastomers with irregular geometries under arbitrary boundary conditions. However, many parameters may be needed to characterize any given industrial material,[19] so that these nonlinear field theories are difficult to use in applications.

This paper introduces an experimental setup to measure the swelling pressure as a function of time. To analyze these experimental data, we derive a time-relaxation equation from the linear poroelastic theory. We determine the diffusivity by fitting the model with experimental results. We observe that diffusivity increases linearly with swelling ratio. The experiments and model together provide an approach to characterize the kinetics of swelling under constraints.

II. EXPERIMENTS

In the experiment, a dry cylindrical sample is initially tightly fit into a metallic tube with two porous ceramic disks on its top and bottom (Fig. 1). The bottom disk is fixed, while a compression tester is linked to the top disk, recording the contact pressure generated by the sample. The whole sample is then submerged into a solvent bath with temperature maintained at 82 °C. The constrained swelling ratio is controlled by the gap between the two disks. This setup is inspired by Katti and Shanmugasundaram,[20] and here we add a thermal bath to control the temperature. We design this experimental setup to resemble the real application, where elastomer is constrained by rock or cement, and the solvent comes from the crevices, cracks or gaps.

In this experimental setup, the metallic tube (internal diameter 29 mm and external diameter 50 mm) is made of stainless steel, which is much stiffer than the elastomer. The sample consists of 6 stacked rubber disks (total thickness 12 mm) cut from sheets (molded following ASTM D3182). The diameter of the rubber disks is 29 mm, which is identical to the internal diameter of the metallic tube, so that the rubber disks will not swell in the radial direction. The ceramic disks (diameter 29 mm and height 13 mm) are cut from sintered ceramic plaques consisting of aluminum oxide with connected porosity and an average pore size of 90 μm, which guarantees that the permeation of the solvent through the plate is much faster than the permeation of the solvent through the elastomer. The solvent bath is heated using an

a)Email: ylou@slb.com

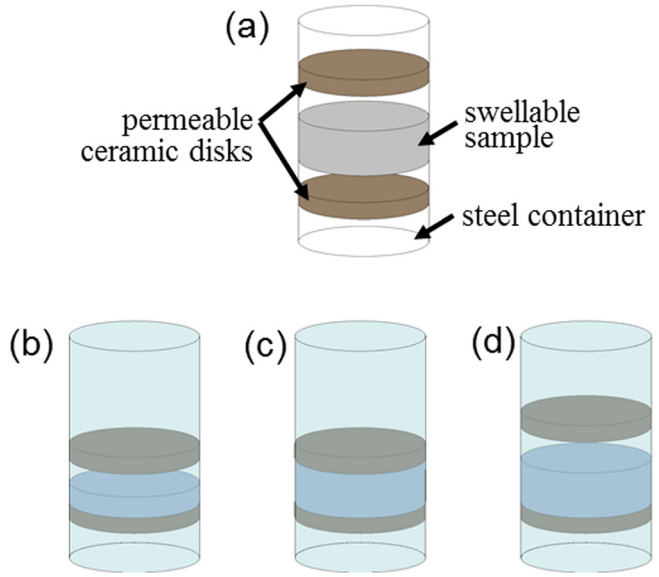

FIG. 1. Schematic of experimental setup and procedure, where (a) illustrates the major components and their relative locations for this experiment, (b) shows the initial step of this experiment, in which a gap is placed between the sample and the top disk, (c) shows after touching the top disk, the swelling of the sample is constrained triaxially, and (d) shows after the swelling reach equilibrium, the top disk is adjusted to a higher location for the next step.

electric resistance placed at the bottom of the device, with the temperature kept homogeneously at $82 \pm 2\,^{\circ}\mathrm{C}$. The compression tester is an INSTRON5569. The 5 kilo Newton load cell on the movable crosshead is connected to a 200 mm long steel shaft that contacts the upper ceramic disk.

At the beginning of the experiment, the cell, which includes metallic tube, sample, porous disks, bath (no solvent has been added yet) and heater, is placed in the INSTRON machine, on a semi-spherical joint. This joint helps to correct misalignments in the setup. The cell is then heated to the set temperature. Once at thermal equilibrium (note that no solvent is added at this moment and the sample is still in air), the gap is adjusted to the desired value, corresponding to the desired swelling ratio, as illustrated in Fig. 1(b). For example, the gap is adjusted to 1.2 mm for the 10% swelling of the 12 mm thick sample. Then, the solvent, pre-heated to $82\,^{\circ}\mathrm{C}$, is added into the cell. The gap is adjusted after thermal equilibrium in air to ensure maximum accuracy, but due to different thermal properties of air and oil, the thermal expansion of the shaft may vary after the introduction of solvent, which may introduce a variation of length on the order of hundred micrometers, i.e., a few percents of error in the swelling ratio. From the moment the sample touch the top disk (Fig. 1(c)), a contact load is generated and being recorded until reaching an asymptotic value. The gap is then increased by moving up the shaft (for example, the shaft is moved up by another 1.2 mm to reach 20% swelling), as illustrated in Fig. 1(d). The test described in this paper lasted around 30 days (4 steps), during which the sample aging is considered negligible.

In this work, a commercially available styrene butadiene polymer (Astlett Rubber SBR 1502) is compounded with regular rubber additives (activators, antioxidants, accelerators) and sulfur cured. It is compounded and molded following ASTM D3182 in sheets that have the dimensions $150\,\mathrm{mm} \times 150\,\mathrm{mm} \times 2\,\mathrm{mm}$. The solvent is chosen as hexadecane (99% purity, Sigma Aldrich). This combination is representative of the oilfield application. The test temperature of $82\,^{\circ}\mathrm{C}$ is also characteristic of low temperature oil wells and has the benefit of accelerating the swelling and homogenization processes. The gap has been set from 10% to 40% of the original sample height, with 10% as the interval. This swelling ratio range is representative of swelling ratios expected in oilfield applications.

III. KINETICS OF SWELLING PRESSURE BUILDUP

Using the experimental setup mentioned above, we have measured the kinetics of swelling pressure buildup at different swelling ratios (10%, 20%, 30%, and 40%) and results are shown in Figs. 2 and 3. The curve for the swelling ratio 40% displays a small jump at round 1 day, which we think is related to misalignment correction due to the semi-spherical joint movement.

After touching the top disk (Fig. 1(c)), the swelled sample is constrained in radial direction by the metal tube and axle direction by top and bottom ceramic disks. At the moment of touching, the solvent is concentrated near the top and bottom surface and the contact load (swelling pressure) is zero. Associated with the redistribution of the solvent inside, the swelling pressure tends to increase and reach maximum when equilibrium state reaches.

The kinetics of swelling pressure buildup is studied using a linear poroelastic theory. This theory is adapted from Biot's theory for the consolidation of soil[21] and has been shown to agree well with experiment of the constrained swelling of a hydrogel thin layer.[22] By assuming the solvent concentration is uniform over the cross-section of the sample, this linear poroelastic problem becomes one-dimensional and the time-evolution of solvent concentration, displacement fields and the swelling pressure can be obtained analytically as a series of Fourier expansion. Detailed discussion is given in the Appendix. The leading term of the analytical solution for swelling pressure is given as

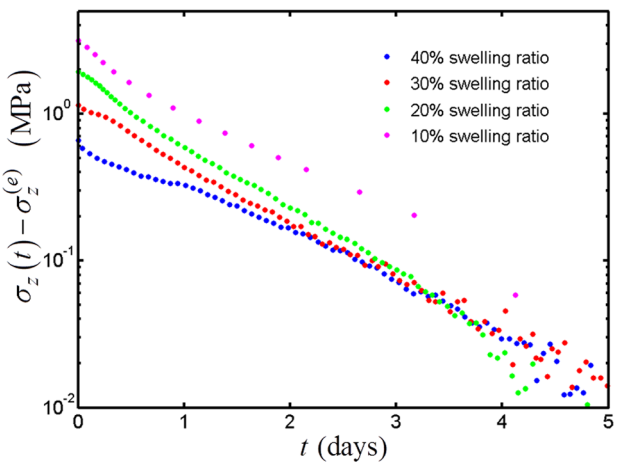

FIG. 2. Semi-logarithmic plot between $\sigma_z(t) - \sigma_z^{(e)}$ and the time t.

TABLE I. Coefficient values obtained from four steps of experiments.

V/V_o	$\sigma_z^{(e)}$ (MPa)	τ (10^4s)	D (10^{-11}m^2/s)
1.1	−3.14	7.50	2.05
1.2	−1.92	7.50	2.44
1.3	−1.18	9.02	2.38
1.4	−0.75	10.00	2.50

$$\sigma_z(t) = \sigma_z^{(e)}\left[1 - \exp\left(-\frac{t}{\tau}\right)\right], \tag{1}$$

where $\sigma_z^{(e)}$ is the equilibrium swelling pressure that is taken as the long-time value measured from experiments, and τ is given by

$$\tau = H^2/(4\pi^2 D) \ . \tag{2}$$

Here H is the distance between the top and bottom disks (the height of the sample after swelling) and D is the diffusivity of the solvent inside elastomer. Therefore, the development of swelling pressure can be considered as a time-relaxation process and τ is the time-scale to reach equilibrium.

First, we demonstrate that the swelling pressure as a function of time measured from experiments is well represented by this time-relaxation form. Equation (1) can be rewritten as

$$\log[\sigma_z(t) - \sigma_z^{(e)}] = \log\left(-\sigma_z^{(e)}\right) - \frac{t}{\tau}. \tag{3}$$

This expression is a semi-logarithmic relation between $\sigma_z - \sigma_z^{(e)}$ and t. The experimental data are plotted in this form in Fig. 2. After a short transitional period (around 1 day), $\log[\sigma_z(t) - \sigma_z^{(e)}]$ decreases nearly linearly with respect to t until reaching equilibrium (after 4 days). Therefore, the buildup of swelling pressure is indeed a time-relaxation process as predicted by the linear poroelastic theory.

Next, we extract the diffusivity D. According to Eq. (3), the slops of the lines in Fig. 2 correspond to the characteristic time τ. These slops, together with Eq. (2), determine the values of D for different swelling ratios, as listed in Table I. Fig. 3 compares the time-relaxation curves with the coefficient values specified in Table I (solid blue lines) and the experimental results (red dots). The fitting curves are in good agreement with those measured experimentally, especially after short transitional periods. This agreement further

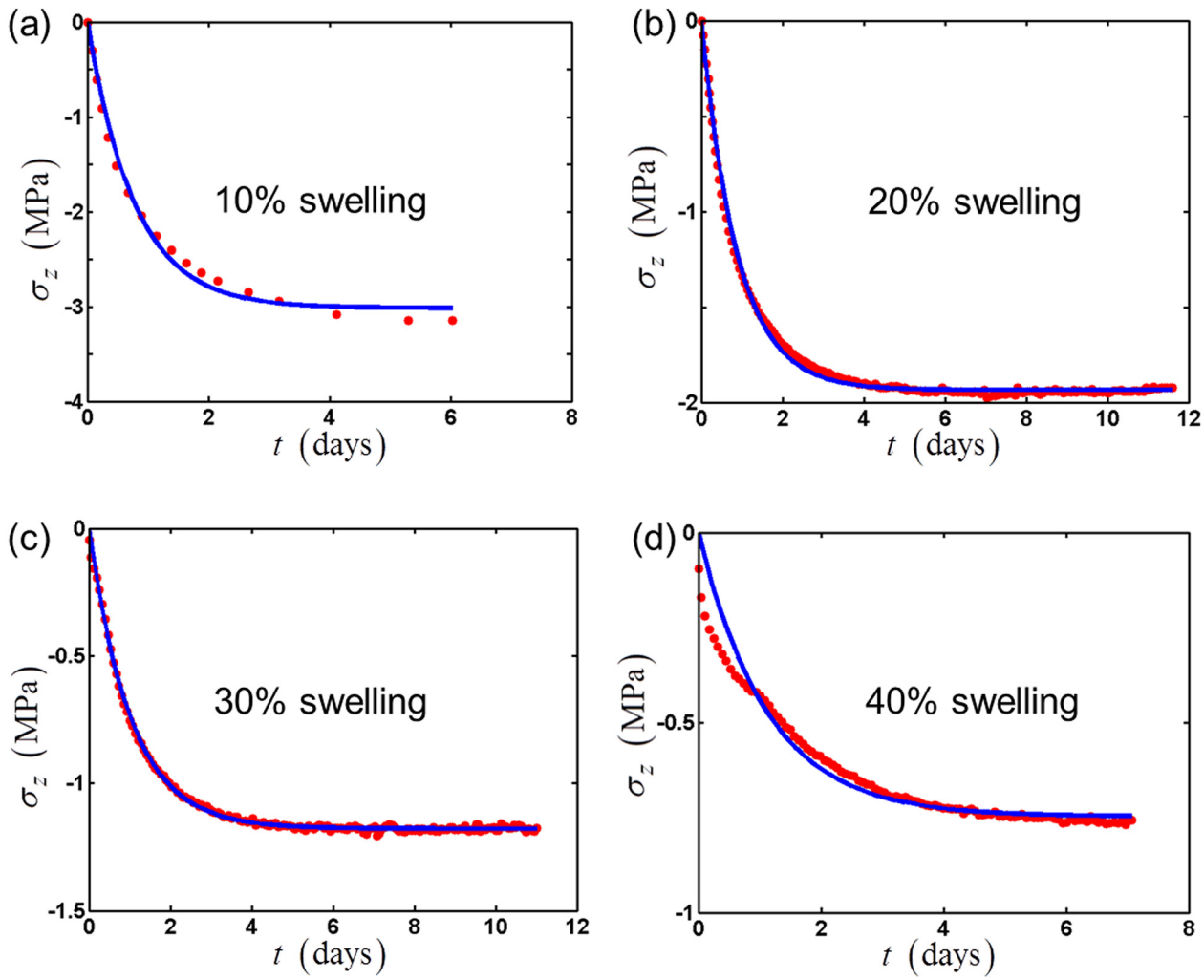

FIG. 3. The comparison between the experimental results (red dots) and numerical fitting (solid blue line), where (a)–(d) are results for swelling ratios changed from 10% to 40%.

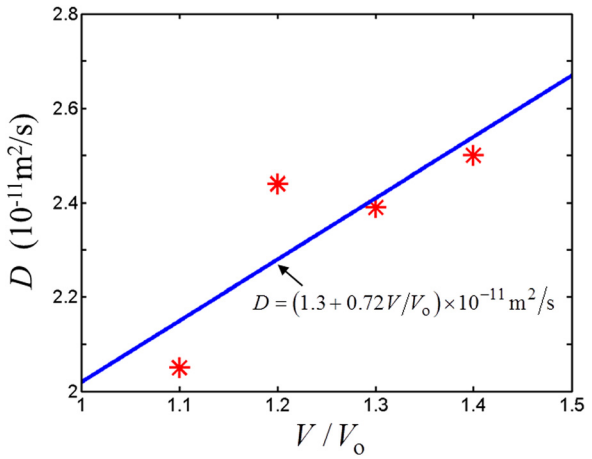

FIG. 4. Correlation between diffusivity and swelling ratios, where the red dots are the diffusivity values extracted from experiments and the straight blue line is the linear fitting between diffusivity and swelling ratios.

corroborates the validity of this method. The diffusivities estimated for each case are shown to have a positive correlation with the swelling ratio, as shown in Figure 4. This trend can be approximated with a linear relation using least-square fitting

$$D\left(\frac{V}{V_o}\right) = D_o + \Delta D\frac{V}{V_0}, \tag{4}$$

where $D_o = 1.30 \times 10^{-11}\mathrm{m}^2/\mathrm{s}$ and $\Delta D = 0.72 \times 10^{-11}\mathrm{m}^2/\mathrm{s}$. It has been reported that the diffusivity increases with swelling ratio,[23] which is consistent with the observation made in this work.

IV. CONCLUSION

This paper introduces an experimental setup to measure the swelling pressure as a function of time. The elastomer swells under triaxially constrained conditions, which are representative of oilfield applications. A simple time-relaxation form that is developed from the linear poroelastic theory is demonstrated to be able to readily capture the kinetics of swelling pressure buildup measured from experiments. By fitting the theoretical expression to the experimental data, we obtain the effective diffusivity of the solvent in the elastomer. The effective diffusivity is found to increase with the amount of swelling. The experimental setup developed here, along with the method to analyze data, can be applied to other swellable elastomers of interest.

APPENDIX: LINEAR THEORY ON SWELLING UNDER CONSTRAINT

The linear model of swellable elastomers[22,24] is adapted from Biot's poroelastic theory for the consolidation of soil. In this work, this model is used to study the buildup of swelling pressure measured from the experiments. An elastomer imbibes a solvent and forms a body. In the reference state, the body is subject to no mechanical load, the concentration of the solvent in the body is C_o, and the chemical potential of the solvent in the body is μ_o. In the current state, the body deforms by displacement field u_i, the chemical potential of the solvent in the environment is μ, and the stresses are given by

$$\sigma_{ij} = 2G\left(\varepsilon_{ij} + \frac{\nu}{1-2\nu}\varepsilon_{kk}\delta_{ij}\right) - \frac{\mu-\mu_0}{\Omega}\delta_{ij}, \tag{A1}$$

where $\varepsilon_{ij} = 1/2(u_{i,j} + u_{j,i})$ are the strains, G is the shear modulus, ν is Poisson's ratios, and Ω is the molar volume of the solvent. Since the volume of mixing swellable elastomer and the corresponding solvent is often negligible comparing to the deformation, we apply the molecular incompressible condition[25,26]

$$\varepsilon_{kk} = (C - C_0)\Omega, \tag{A2}$$

where C is the solvent concentration in the current state. In each moment, the body is always in force balance

$$\sigma_{ij,j} = 0. \tag{A3}$$

However, the solvent in the different parts of the body may not be in equilibrium, so that the solvent can migrate in the body. The conservation of the number of solvent molecules requires that

$$\frac{\partial C}{\partial t} + \frac{\partial J_k}{\partial x_k} = 0, \tag{A4}$$

where J_k is the flux of the solvent in the body. We will assume that the flux obeys Darcy's law

$$J_i = -\left(\frac{k}{\eta\Omega^2}\right)\frac{\partial \mu}{\partial x_i}, \tag{A5}$$

where k is the permeability and η is the viscosity of the solvent. A combination of the above equations gives that

$$\frac{\partial C}{\partial t} = D\frac{\partial^2 C}{\partial x_k \partial x_k}, \tag{A6}$$

with

$$D = \frac{2(1-\nu)Gk}{(1-2\nu)\eta}. \tag{A7}$$

Substituting Eq. (A1) into Eq. (A3) gives

$$G\Omega\left(\frac{\partial^2 u_i}{\partial x_k \partial x_k} + \frac{1}{1-2\nu}\frac{\partial^2 u_k}{\partial x_k \partial x_i}\right) = \frac{\partial \mu}{\partial x_i}. \tag{A8}$$

Substituting Eq. (A2) into Eq. (A6) gives

$$\frac{\partial}{\partial t}\frac{\partial u_i}{\partial x_i} = D\frac{\partial^3 u_i}{\partial x_k \partial x_k \partial x_i}. \tag{A9}$$

Therefore, the displacement field $u_i(x_i, t)$ and chemical potential field $\mu(x_i, t)$ are governed by Eqs. (A8) and (A9) together.

In the experiment described in this work, the swelling of the sample involves two sequential processes: before and after touching the top disks. Initially, the sample is only constrained laterally and can swell freely in the axle (z) direction. Therefore, the top surface of the sample is stress-free and has identical chemical potential with the outside solvent. When the top surface touches the top disk, the displacement of the top surface of the sample becomes fixed. This experimental procedure is designed to mimic the sealing of swellable packers, e.g., the packer will first touch the wellbore then gradually build up the swelling pressure.[27] In this work, we will focus on the second process, i.e., the buildup of swelling pressure after sealing. The analysis of the first process, i.e., one-dimensional free-swelling, can be found in the literature[17] and will not be discussed here.

For simplicity, we assume that the deformation and chemical potential are homogenous over the cross-section of the sample. Therefore, all the non-zero gradients are along the z direction. Then, integrate Eq. (A9) over z gives

$$\frac{\partial u_z}{\partial t} = D\frac{\partial^2 u_z}{\partial x_z \partial x_z}. \tag{A10}$$

Due to symmetry, only half of the sample is considered, i.e., from the middle surface, defined as $z = 0$, to the surface of the sample, defined as $z = H/2$, where H is the distance between the top and bottom disks (and the height of the sample after swelling). After the sample is in contact with the top constraints, the boundary conditions are specified as

$$\begin{aligned} &u_z(0,t) = 0, \quad \partial u_z/\partial z(0,t) = 0, \\ &u_z(H/2,t) = \Delta H/2, \quad \mu(H/2,t) = \bar{\mu}, \end{aligned} \tag{A11}$$

where ΔH is the gap between sample and top disk before swelling and $\bar{\mu}$ is the chemical potential of the outside solvent. The governing equations (A8) and (A10) with boundary conditions (A11) and any given initial conditions form a well-stated boundary value problem. The Fourier-type analytical solutions for this problem can be expressed as

$$u_z(z,t) = \frac{\Delta H}{H}z + \sum_{n=1}^{\infty} M_n \exp\left(-\frac{n^2 t}{\tau}\right)\sin\left(\frac{2n\pi z}{H}\right), \tag{A12}$$

where M_n are the coefficients that can be determined from initial conditions.

In one-dimensional case, the constitutive relation (A8) can be simplified as

$$\sigma_z = 2G\frac{1-\nu}{1-2\nu}\frac{\partial u_z}{\partial x_z} - \frac{\mu - \mu_0}{\Omega}. \tag{A13}$$

Since the stress is uniform throughout the sample, we can calculate σ_z at the top surface. Substituting Eq. (A12) into Eq. (A13) with $\mu = \bar{\mu}$ and $z = H/2$ gives

$$\begin{aligned} \sigma_z(t) = {} & 2G\frac{1-\nu}{1-2\nu}\left[\frac{\Delta H}{H} + \sum_{n=1}^{\infty}\frac{2n\pi}{H}(-1)^n M_n \exp\left(-\frac{n^2 t}{\tau}\right)\right] \\ & - \frac{\bar{\mu} - \mu_0}{\Omega}. \end{aligned} \tag{A14}$$

The equilibrium stress, $\sigma_z^{(e)}$, can be obtained by taking $t \to \infty$ in Eq. (A14), which gives

$$\sigma_z^{(e)} = 2G\frac{1-\nu}{1-2\nu}\frac{\Delta H}{H} - \frac{\bar{\mu} - \mu_o}{\Omega}. \tag{A15}$$

Therefore, the expression for σ_z can be re-written as

$$\sigma_z(t) = \sigma_z^{(e)}\left[1 - \sum_{n=1}^{\infty} m_n \exp\left(-\frac{n^2 t}{\tau}\right)\right], \tag{A16}$$

where m_n is defined as

$$m_n = 4G\frac{1-\nu}{1-2\nu}\frac{n\pi}{H}(-1)^{n+1}\frac{M_n}{\sigma_z^{(e)}}. \tag{A17}$$

If the initial state is taken as the moment when sample touches the top disk, then we substitute $\sigma_z(0) = 0$ into Eq. (A16) and obtain

$$\sum_{n=1}^{\infty} m_n = 1 \quad . \tag{A18}$$

Since the exponential terms with large n in Eq. (A16) decays rapidly with the increase of time t, we can anticipate that the time evolution of swelling pressure will be captured by first few terms after a short transitional period. For simplicity, we only consider the first term and modify the condition (A18) to be $m_1 = 1$. The buildup of swelling pressure given by Eq. (A16) is simplified as

$$\sigma_z(t) = \sigma_z^{(e)}\left[1 - \exp\left(-\frac{t}{\tau}\right)\right], \tag{A19}$$

which is the time-relaxation form given by Eq. (1).

[1] P. Cavanagh, C. R. Johnson, S. LeRoy-Delage, G. DeBrujin, I. Cooper, D. Guillot, H. Bulte, and B. Dargaud, in *SPE/IADC Drilling Conference, Amsterdam*, The Netherlands, 20–22 February 2007, Paper No. SPE/IADC105781.

[2] N. Moroni, N. Panciera, A. Zanchi, C. R. Johnson, S. LeRoy-Delage, H. Bulte-Loyer, S. Cantini, and E. Belleggia, in *SPE Annual Technical Conference and Exhibition*, Anaheim, California, US., 11–14 November 2007, Paper No. SPE 110523.

[3] J. Roth, C. Reeves, C. R. Johnson, G. De Bruijn, M. Bellalarba, S. LeRoyDelage, and H. Bulte-Loyer, in *IADC/SPE Drilling Conference*, Orlando, Florida, US., 4–6 March 2008, Paper No. IADC/SPE 112715.

[4] M. Kleverlaan, R. H. van Noort, and I. Jones, in *SPE/IADC Drilling Conference, Amsterdam*, The Netherlands, 23–25 February 2005, Paper No.SPE/IADC 92346.

[5] V. Fjellatad, R. Berbkvam, and T. Li, Hart's E&P **79**, 79 (2006).

[6] M. S. Laws, J. E. Fraser, H. F. Soek, and N. Carter, in *Asia Pacific Drilling Conference and Exhibition*, Bangkok, Thailand, 13–15 November 2006, Paper No. IADC/SPE 100361.

[7] D. Hembling, S. Salamy, A. Qatani, N. Carter, and S. Jacob, in *Drilling Contractor*, September/October, 2007, pp. 108–114.

[8] E. B. Nelson and D. Guillot, *Well Cementing*, 2nd ed. (Schlumberger, 2006), p. 220.

[9] M. E. Jordan and R. A. Shepherd, *SPE Annual Technical Conference and Exhibition*, 22–26 September 1985, Las Vegas, Nevada.

[10] A. S. Al-Yami, H. A. Nasr-El-Din, M. Z. Awang, A. S. Al-Humaidi, and M. K. Al-Arfaj, *International Petroleum Technology Conference (IPTC)*, 3–5 December 2008, Kuala Lumpur, Malaysia.

[11]A. S. Al-Yami, H. A. Nasr-El-Din, and A. S. Al-Humaidi, *SPE Asia Pacific Oil and Gas Conference and Exhibition*, 20-22 October 2008, Perth, Australia.
[12]C. Wang, Y. Li, and Z. Hu, Macromolecules **30**, 4727 (1997).
[13]I. J. Suarez, A. Fernandez-Nieves, and M. Marquez, J. Phys. Chem. B **110**, 25729 (2006).
[14]M. Doi, J. Phys. Soc. Jpn. **78**, 052001 (2009).
[15]W. Hong, X. H. Zhao, J. X. Zhou, and Z. G. Suo, J. Mech. Phys. Solids **56**, 1779 (2008).
[16]J. Dolbow, E. Fried, and H. Ji, J. Mech. Phys. Solids **52**, 51 (2004).
[17]W. Hong, Z. S. Liu, and Z. G. Suo, Int. J. Solids Struct.**46**, 3282 (2009).
[18]S. A. Chester and L. Anand, J. Mech. Phys. Solids. **58**, 1879 (2010).
[19]Y. Lou, A. Robinsson, S. Cai, and Z. Suo, J. Appl. Phys. **112**, 034906 (2012).
[20]D. R. Katti and V. Shanmugasundaram, Can. Geotech. J. **38**, 175 (2001).
[21]M. A. Biot, J. Appl. Phys. **12**, 155 (1941).
[22]J. Yoon, S. Cai, Z. Suo, and R. C. Hayward, Soft Matter **6**, 6004 (2010).
[23]L. Masaro and X. X. Zhu, Prog. Polym. Sci. **24**, 731 (1999).
[24]Y. Hu, X. Chen, G. M. Whitesides, J. Vlassak, and Z. Suo, J. Mater. Res. **26**, 785 (2011).
[25]B. E. Eichinger and P. J. Flory, Trans. Faraday Soc. **64**, 2053 (1968).
[26]N. V. Sastry and M. C. Patel, J. Chem. Eng. Data **48**, 1019 (2003).
[27]S. Cai, Y. Lou, P. Ganguly, A. Robisson, and Z. Suo, J. Appl. Phys. **107**, 103535 (2010).